Chapter 5
Surface Hardening on Wheel Steel Using Electrolytic Plasma: Formation of Fine Structure and Phase Composition of Wheel Steel Due to Plasma Hardening

Yerkezhan Tabiyeva
https://orcid.org/0000-0002-9726-7187
D. Serikbayev East Kazakhstan Technical University, Kazakhstan

Bauyrzhan Rakhadilov
LLP PlasmaScience, Kazakhstan

Gulzhaz Uazyrkhanova
D. Serikbayev East Kazakhstan Technical University, Kazakhstan

Waqar Ahmed
University of Lincoln, UK

ABSTRACT

Transmission electron microscopy (TEM) investigations of the structure and phase composition of ferritic-pearlitic wheel steel mark two surface after electrolyte-plasma surface hardening are presented. Initially the morphology of the steel matrix consists of lamellar perlite and non-fragmented and fragmented ferrite. Electrolytic plasma quenching of the steel surface results in the martensite transformation, steel self-tempering, and the formation of cementite particles in all martensite crystals. This treatment also leads to the diffusion transformation of gamma to alpha phases, the release of residual austenite along the low-temperature martensite laths and lamellas and in all crystals of lamellar martensite, the formation of M23C6 special carbides and, finally, to the enhancement of all parameters of the steel fine structure.

DOI: 10.4018/978-1-6684-6830-2.ch005

INTRODUCTION

Industrial progress is determined implementation of new technologies that improve the quality of products. Efficient production of machinery is impossible without using new technologies that provide the required combination of strength and plastic properties of constructional steels. Hence, machinery life and performance depend on the wear resistance of parts, which undergo considerable reversing impact loads. The surface layer must possess high strength and hardness combined with sufficient core viscosity. This can be achieved using a variety of the surface hardening techniques (Kondrat'ev et al., 2014; Nguyen et al., 2022; Paulmier et al., 2008; Zhang et al., 2009). An effective method of surface hardening of iron-carbon steels is electrolytic plasma treatment. High-speed heating and cooling in the thermal influence zone, structural changes due to phase transitions provide the operational characteristics of the working surface (Rakhadilov et al., 2016; Rakhadilov et al., 2018). An important feature of plasma hardening is its effective application for additional surface hardening after conventional volumetric thermal treatment. The life and economical use of railway products is related to the strength and tribological properties of products made from wheel steels (Konstantinova et al., 2019; Wang et al., 2003). The pace of economic and social development of society largely depends on the efficiency and quality of railway transport. There is a need to equip railways with modern traction rolling stock with increased reliability of its components, one of which is wheel sets, the tires of which are made of grade 2 wheel steel. At the moment, the problem of wear of wheel sets of traction rolling stock has become especially acute. In this regard, it is effective to increase the reliability and extend the uptime of railway equipment, which, in turn, contributes to the safety of train traffic. To improve the properties of wheel steels, it is necessary to study the influence of surface hardening on the steel structure to achieve the desired mechanical characteristics. This study focuses on phase composition, fine structure and mechanical properties of wheel steel mark 2 before and after electrolyte-plasma surface hardening.

MATERIAL AND METHODS OF RESEARCH

Wheel steel mark 2 was used to fabricate railway wheel sets. In its initial state wheel steel mark 2 represents material exposed to hardening at 890^0C for 2-2.5 hours with cooling in warm water (30-60^0C) followed by temperingat 580^0C for 2.5-3 hours. Steel samples were cut out of the wheel as parallelepiped in size 15×15×10 mm^3. The samples were free from deformation and thermal effect under slow cutting speed and low load. According to GOST 398-96, chemical composition of steel (in %) is C-0.57-0.65; Mn-0.50-0.90; Si-0.22-0.45; V - not exceeded 0.10; S- not exceeded 0.030 and P-not exceeded 0.035 respectively.

Electrolyte-plasma surface hardening in cathode mode was carried out at the electrolyte-plasma treatment plant at the Scientific Research Center "Surface Engineering and Tribology" at the S. Amanzholov East Kazakhstan University (Rakhadilov, Tabieva, & Zhurerova, 2019; Rakhadilov, Tabiyeva, Uazyrkhanova et al, 2019; Tabieva et al., 2020).

Steel structure and phase composition on thin foils were investigated using the EM-125 TEM at 125 kV accelerating voltage, before and after electrolyte-plasma surface hardening. The phase identification was carried out using TEM, microdiffraction patterns and dark-field images obtained in the respective reflections. TEM images of the fine steel structure were used for the structure morphology classification, phase identification and localization, and determination of such parameters as scalar and excess disloca-

Figure 1. Process of processing of an electrolyte plasma sample (a) and functional diagram (b) of the machine 1– in-process part; 2 – conic stainless steel electrolytic cell; 3– bottom plate; 4–pump; 5– heat exchanger; 6– bath filled with electrolyte

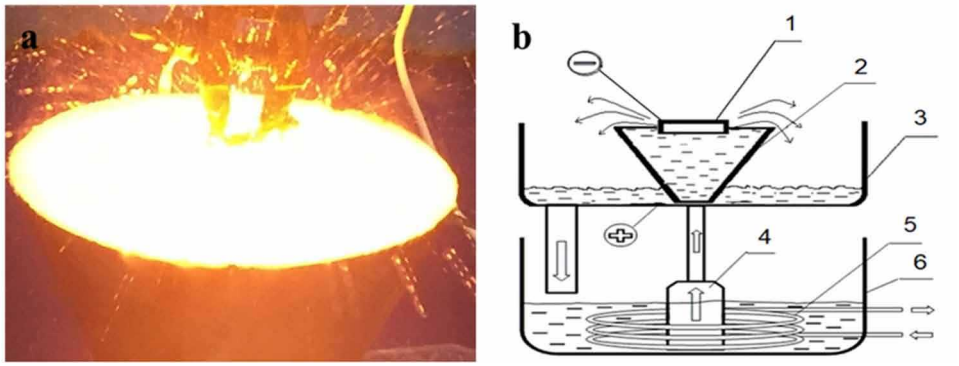

tion density, bending-torsion amplitudes of the crystal lattice, and internal stress amplitude for the fine steel structure. All the parameters were calculated using standard procedures. The surface morphology was studied on the scanning electron microscope JSM-6390LV, equipped with the energy-dispersive analysis prefix INCA Energy Penta FET X3. The microstructure was studied using an Altami MET-1M optical metallographic microscope in reflected light at a light field. The microhardness was measured in PMT-3M machine in accordance with GOST 9450-76, with loads of 100g and holding time for 10 seconds. Electrolyte-plasma surface hardening (EPSH) of the steel was carried out in the cathode mode in electrolyte-plasma treatment machine (Rakhadilov et al.,), scheme (Figure 1a) and processing (Figure 1b). High-current rectifier with output power of 360V/60A as was used as a power source. The samples were processed by rapid heating for 2 seconds followed by cooling in a flowing electrolyte. The process used the following parameters: electrolyte composition (%, mass): 10% urea $(NH_2)_2CO$ + 20% sodium carbonate Na_2CO_3+70% water, processing lasted for 2 seconds, T_{max} = 850-900°C; U= 320V; I=40A.

RESULTS AND DISCUSSION

Microstructural of the near-surface layers of wheel steel mark 2 samples subjected to electrolyte-plasma surface quenching in electrolyte plasma showed structural changes. Figure 2 shows the microstructures

Figure 2. Microstructure of Wheel Steel Mark 2 before and after electrolyte-plasma surface hardening obtained by Optical metallographic microscope a) initial state; after electrolyte-plasma surface hardening: b) 1 s, c) 2 s, d) 3 s, e) 4 s

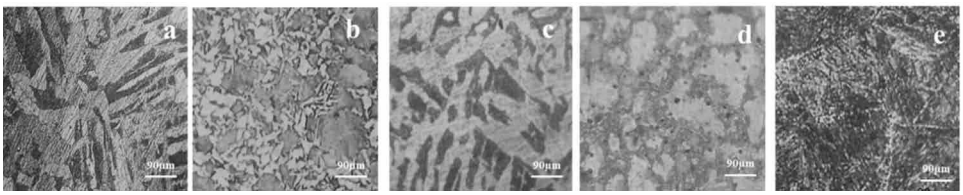

Figure 3. X-ray phase analysis of Wheel Steel Mark 2 a) initial state, b) after electrolyte-plasma surface hardening

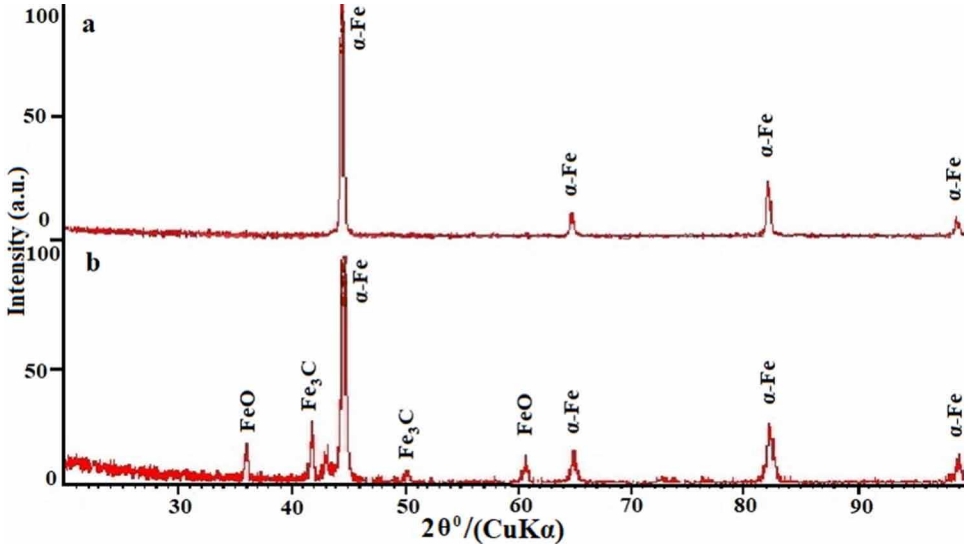

of the surface layer of steel before and after hardening at processing time of 1,2,3,4 seconds at a temperature of 850-900°C.

After electrolyte-plasma surface hardening for 3-4 seconds, the growth of the ferritic structure was observed, while the grains of perlite decrease. After electrolyte-plasma surface hardening with heating for 2 seconds, the formation of a cementite mesh is observed in the structure of wheel steel mark 2, which is located around the ferrite. X-ray diffraction analysis in Figure 3 shows that iron oxide was found along with cementite. This is explained by the fact that the oxygen concentration on the surface is not high enough, as well as the content of carbamide in the composition of the electrolyte prevents the formation of a continuous oxide layer, so it is more correct to say the surface layer contains iron oxide, which does not affect the further characteristics of the steel after EPSH. The grains of the perlite phases decrease gradually compared to the microstructure of wheel steel mark 2 before EPSH. Thus, the microstructure of the surface of the hardened steel sample is a fine-grained ferrite structure.

Tribological properties of the samples before and after electrolyte-plasma hardening were also investigated.

Experimental curves of the dependence of the coefficient of friction on the length of the runare shown (Figure 4). The test was carried out according to the "ball-disc" scheme, the length of the run was 31m, the speedwas 2cm/s, theloadwas 5N.

Test results showed that the average friction coefficients at a normal force of 5N and a mutual displacement velocity of 2cm/s are in the range from 0.27 to 0.40, which possibly indicates the destruction of the surface layer of the samples. All processed samples have a good degree of improvement in tribological properties. The results of experimental studies on structural-phase state of wheel steel mark 2 showed that in its initial state the steel matrix represents α-phase - solid solution of carbon and alloying elements in α-Fe with BCC matrix. Lamellar pearlite and ferrite are morphological components of α-phase. Lamellar perlite, almost ideal, i.e., it is a conglomerate of alternating parallel plates ferrite and cementite (Kozlov et al., 2014). Ferrite (α-phase) in the pearlite has a volumetric-centered cubic (BCC) crystal lattice. Mutual

Figure 4. Coefficient of friction of Wheel Steel Mark 2 before and after electrolyte-plasma surface hardening: (b) initial; (c) 2 s; (d) 3 s; (e) 4 s

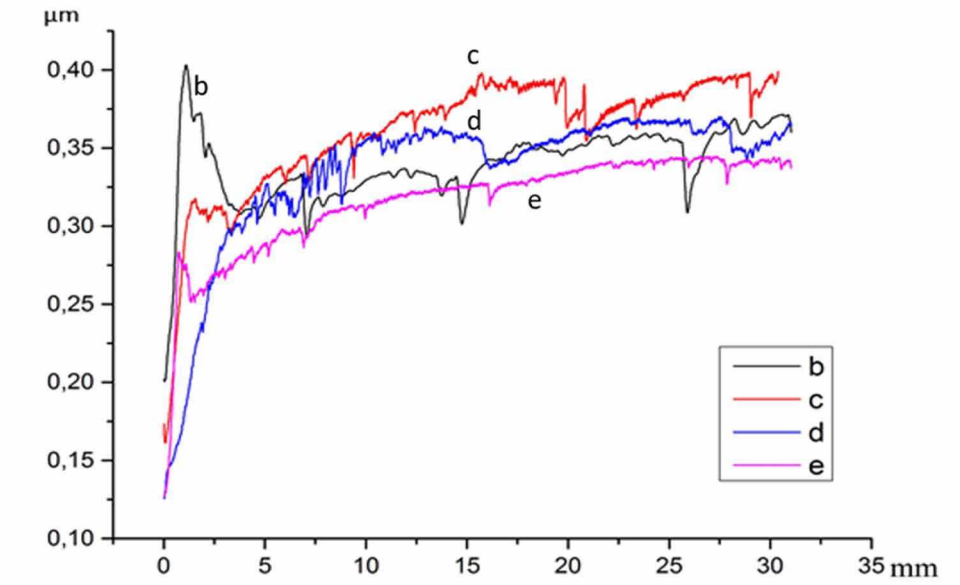

parallelism of the lamellas (Abuali & Mousavi, 2013) means that, firstly, different lamellas of the same phase within the colony have the same orientation and, secondly, mutual orientation of two phases (their orientation ratio) provides best coupling of two crystal lattices along the habit surface of the lamellas. It is established (Skakov et al., 2013) that Bagaryatsky orientation relationship is observed between ferrite and cementite in nearly every pearlite colony, which is not related to the carbon content in the steel. It should be noted that steel alloying does not affect the crystallographic characteristics within the pearlite (Rakhadilov et al., 2020). The volume ratio of lamellar pearlite is 35% along the material (Table 1). It should be noted that the planning method was used to determine the volume fraction, which is reduced to the measurement of the total area of sections of this structural component on a certain area of the foil. The conclusion of this method is based on the principle of Cavalieri-Anker-Glagolev. It postulates the relationship between the Area (P_S) and Volume (P_V) shares:

$$P_V = P_S, \tag{1}$$

This is one of the fundamental relationships of stereology was postulated by S.A. Saltykov [17;51]. The formula has the following form:

$$P_S = \frac{S}{L^2} = \frac{V}{L^3} = P_V, \tag{2}$$

Where S and V are the area and volume occupied by the corresponding structural component in the sample element representing the L-rib cube.

Ferrite in the initial state of the wheel steel mark 2 is present in the form of non-segmented and fragmented ferrites. The volume share of non-segmented ferrite is ~10%. The volume of fragmented ferrite is 55%. The surface hardening carried out resulted in the formation of packet-plate martensite. The volume share of pacts of martensite is 60%, plate low-temperature martensite is 10%, plate high-temperature martensite is 30%. Martensite transformation does not take place completely due to residual austenite (γ phase). The crystal lattices of residual austenite and the α-phase, regardless of the type and location of residual austenite, are always interconnected by the Kurdyumov–Sachs orientation relation. The volume fraction of residual austenite (γ-phase) in lath martensite is 6.5%. Studies have shown that in wheel steel mark 2 after surface hardening inside all crystals of martensite's there are particles of cementite. Crystalline grates of cement and α-phase are connected among themselves by the orientation ratio of Bagaryatskiy. The volume fraction of cementite in lath martensite is 0.27%, in low–temperature lamellar martensite is 0.95% and in high-temperature lamellar martensite is 2%. (Table 1). The volume fraction of cement (δ_{FeC}) was calculated using:

$$\delta_{Fe_3C} = \frac{V_{Fe_3C}}{t \cdot r^2}, \tag{3}$$

Where V_{Fe_3C} - average volume of one particle of cement, t - thickness of the foil, r - average distance between particles.

Figure 5 shows that in the initial state, wheel steel mark 2 is a ferrite-perlite mixture and that cementite particles have a lamellar shape, are located almost parallel. There are clear reflexes on the microdiffraction pattern (Figure 5b), which are identified (Figure 5c) like cementite reflexes. The black arrow (Figure 5) indicates the coinciding directions $[011]_\alpha \parallel [21\bar{1}]$ at the same time $(13\bar{3})_\alpha \parallel (1\bar{2}0)_C$ – the Bagaryatsky ratio. The dislocation structure in perlite and ferrite represents close dense dislocation networks. Table 1 shows the highest scalar dislocation density belongs to fragmented ferrite, and the lowest – to the α-phase of lamellar perlite. The mean value of scalar dislocation density in steel is $2.5 \cdot 10^{10}$ cm^{-2}. The dislocation structure of all the morphological components is polarized, i.e., dislocations in the material are mostly excess (Popova, Nikonenko, Tabieva, Uazyrkhanova et al, 2020). This is indicated by the presence of bend extinction contours in the bulk material. Based on the size of the bend extinction contours in each morphological component and in the bulk material, the following quantitative parameters are calculated for the fine structure: bending-torsion amplitude of the crystal lattice, excess dislocation density and amplitude of long-range internal stresses caused by the excess dislocation density. Using the scalar dislocation density, we can calculate the amplitude of internal shear stresses induced by the dislocation structure known as forest dislocations. Table 1 shows that fragmented ferrite is characterized by the highest quantitative parameters, while perlite possess the lowest. The conditions of $\rho > \rho_{\pm}$ and $\sigma_{sh} > \sigma_l$ are satisfied for the whole material. This means that the lattice bending-torsion (distortion) of the wheel steel in the initial state is plastic and does not lead to the steel microcracking (Popova, Nikonenko, Tabieva, & Uazyrkhanova, 2020).

Electrolyte-plasma quenching results in martensite transformation, i.e., the formation of lath and lamellar (low- and high-temperature martensite) (Lobanov et al., 2016). Lath martensite (Figure 6a) is a structural formation comprising a number of elongated laths parallel to each other, which form a packet. Lath martensite probably generates from fragmented ferrite. This is supported by the 60% volume fraction of lath martensite i.e. it is the same as the volume fraction of fragmented ferrite in the initial state.

Table 1. Mean quantitative parameters of perlite and ferrite fine structure and bulk material in the initial state

Morphological Components	Mean Quantitative Parameters of Fine Structure					
	P_V, %	ρ, cm^{-2}	$\rho_{\pm}$, cm^{-2}	χ, cm^{-1}	σ_{sh}, MPa	σ_l, MPa
Perlite	35	2.1×10^{10}	1.4×10^{10}	360	285	240
Nonfragmented ferrite	10	2.6×10^{10}	1.5×10^{10}	365	320	240
Fragmented ferrite	55	2.9×10^{10}	2.8×10^{10}	690	340	330
Bulk material	100	2.5×10^{10}	2.1×10^{10}	525	315	285

Notation: P_V – volume fraction, ρ – scalar dislocation density, $\rho_{\pm}$ – excess dislocation density, χ– bending-torsion amplitudes of the crystal lattice, σ_{sh}– shear stress, σ_l – long-range stress.

Figure 5. Electron microscopic image of the fine structure of the initial state of Wheel Steel Mark 2 obtained by Transmission Electron Microscope a – is a light-field image (LP- lamellar pearlite, FF - fragmented ferrite); b – is a micro-diffraction pattern obtained from the area marked on (a) with a circle; c – is its indexed scheme containing the reflexes of the x-phase and cementite

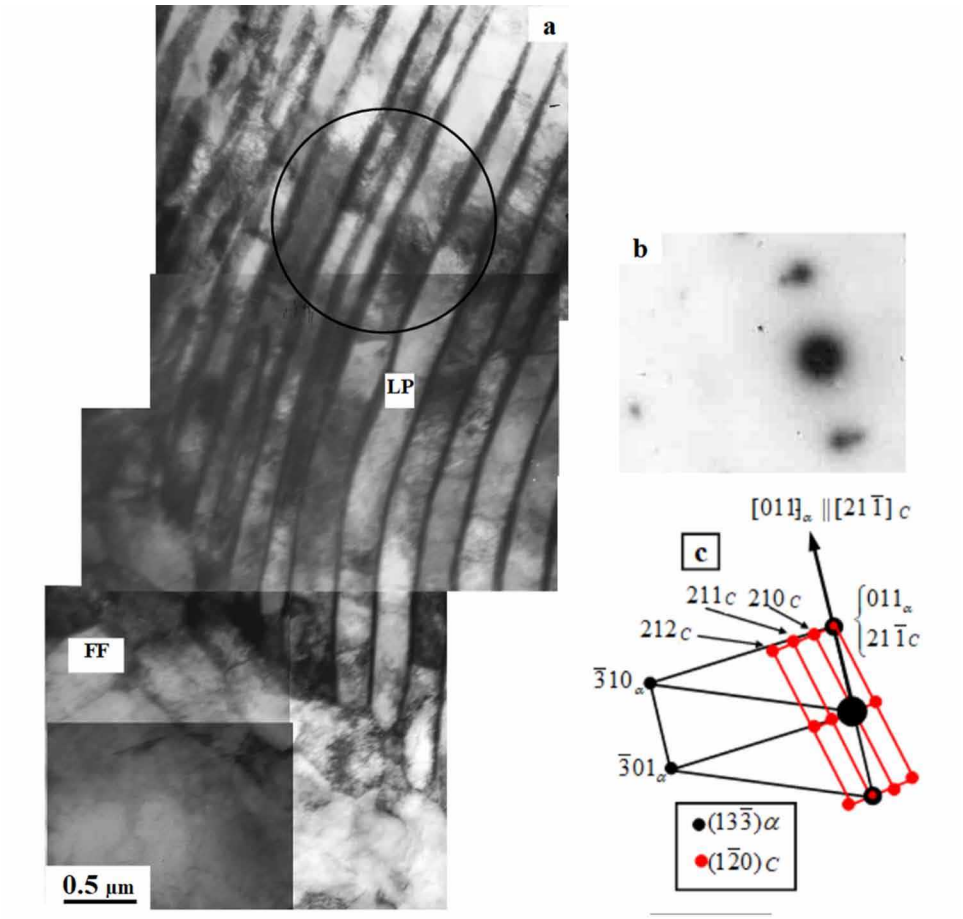

Figure 6. Electron microscopic image of the fine structure of the sample surface after electrolyte-plasma surface hardening obtained by transmission electron microscope

Figure 6 shows a electron microscopic image of the fine structure of the surface of wheel steel mark 2 after electrolyte-plasma surface hardening. In this section, an image of a lath-lamellar or packet-plate martensite is visible: a – a light–field image (LM- lath (packet) martensite, HL-high-temperature lamellar martensite); b, c – microdifraction pattern and its scheme obtained from the area marked on (a) with a dashed line circle; d - the indicated microdifraction pattern obtained from the area marked on (a) with a dashed line with dots circle; e, f – microdifraction pattern and its scheme obtained from the area marked on (a) with a black circle.

Low-temperature lamellar martensite presented in Figure 6a, has the volume fraction of 10%; it is rather large, separately located martensite crystals (laths) having the dislocation structure. In comparison with the initial steel state, low-temperature lamellar martensite probably generates from non-fragmented ferrite, the amount of which is also 10%. High-temperature lamellar martensite presented in Figure 6a, has the volume fraction of 30%; it is large, separately located martensite crystals (laths) propagating through the whole grain and crystals of an arbitrary shape, without a well-defined faceting and grain boundaries. This martensite type probably results from lath perlite. Our findings show the surface hardening results

not only in the martensite transformation, but also in the formation of residual austenite (α-phase) having a face centered cubic crystal system. In lath martensite, residual austenite is present as long thin layers on the boundaries of the martensite laths. In low-temperature lamellar martensite, it represents both long thin layers on the boundaries and aciculae inside the lamellas which constitute the twin-type colonies. In high-temperature lamellar martensite, residual austenite is present in the form of aciculae also forming the twin-type colonies. Our early research (Kashchenko et al., 2012) showed that in lath and lamellar martensite, both low- and high-temperature, Fe_3C particles (self-tempering martensite) appear already during the quenching process. This leads to the formation of carbide particles, viz. cementite inside martensite crystals. Cementite particles generating in self-tempering, are similar to those releasing in steel tempering, namely in shape, localization and crystal geometry. The cementite particle size, the volume fraction and mutual arrangement depend on the martensite type (Rahadilov et al., 2021).

According to our studies, cementite particles observed in all martensite crystals of the wheel steel mark 2 after electrolyte-plasma surface hardening, have a thin lamellar structure and arrange in two and three directions relative to the martensite crystal axis. It is found that the fine cementite particles form in self-tempered lath martensite, while the coarsest ones appear in high-temperature lamellar martensite. The surface quenching process thus leads to martensite transformation and steel self-tempering. Besides cementite, the steel structure contains special carbide $M_{23}C_6$ particles having a cubic crystal lattice. These carbide particles are observed on the boundaries of martensite laths and inside low- and high-temperature lamellar martensite. The analysis shows that special carbide $M_{23}C_6$ particles locating on the boundaries of the martensite crystals, result from the γ-phase. This is confirmed by the fact that the particles are observed inside the residual austenite layers, and the XRD patterns of the martensite crystal boundaries demonstrate the γ -phase reflections along with the reflections of $M_{23}C_6$ carbide. According to the XRD patterns, inside low- and high-temperature lamellar martensite with the twin-type colonies, $M_{23}C_6$ carbide particles are also present in the steel structure. After the surface hardening, $M_{23}C_6$ carbide particles which are not associated with the γ -phase are also found in high-temperature lamellar martensite, on α-phase dislocations. Thus, special carbide $M_{23}C_6$ particles appear due to firstly, decomposition of residual austenite and martensite, secondly, partial dissolution of cementite and, thirdly, carbon moving from α-phase crystal dislocations and boundaries. Thus, in all cases, carbon provides the formation of special carbide $M_{23}C_6$ particles from residual austenite, α-phase solid solution, cementite particles and defects of the crystal lattice. It should be noted that the decomposition intensity of α- and γ-phase solid solutions and the formation of the carbide phase in various structural components of the α -phase (lath martensite, inside low- and high-temperature martensite) are different. They also differ within each structural component. This difference depends on many factors, in particular, the initial state of the material (including the material fragmentation and the type of fragments formed) (Bayatanova et al., 2021).

The dislocation structure of all structural martensite components represents dense dislocation networks. According to Table 2, the highest scalar dislocation density belongs to lath martensite, and the lowest – to high-temperature lamellar martensite. This also confirms that lath martensite results from fragmented ferrite, in which the mean value of scalar dislocation density is the highest, whereas high-temperature lamellar martensite releases from lamellar perlite, in which the mean value of scalar dislocation density is the lowest. The dislocation structure in all structural components of martensite is polarized. This is indicated by the presence of bend extinction contours in all martensite crystals. For each morphological component (lath and low- and high-temperature lamellar martensite) and for the bulk material, the quantitative parameters of the fine structure are calculated before and after the surface quenching, using

Table 2. Mean quantitative parameters of fine structure after electrolytic plasma quenching surface of wheel steel mark two

Morphological Components	Mean Quantitative Parameters of Fine Structure					
	P_V, %	ρ, cm^{-2}	$\rho_{\pm}$, cm^{-2}	χ, cm^{-1}	σ_{sh}, MPa	σ_l, MPa
Lath martensite	60	3.3×10^{10}	2.6×10^{10}	650	365	320
Low-temperature lamellar martensite	10	2.5×10^{10}	1.9×10^{10}	465	315	270
High-temperature lamellar martensite	30	2.3×10^{10}	1.6×10^{10}	410	305	255
Bulk material	100	2.9×10^{10}	2.2×10^{10}	560	340	295
Notation: P_V – volume fraction, ρ – scalar dislocation density, $\rho_{\pm}$ – excess dislocation density, χ– bending-torsion amplitudes of the crystal lattice, σ_{sh} – shear stress, σ_l – long-range stress.						

the values of scalar dislocation density and the size of bend extinction contours. These parameters are summarized in Table 2.

As can be seen from Table 2, the highest quantitative parameters belong to lath martensite, and the lowest belong to high-temperature lamellar martensite. Electrolytic plasma quenching of the steel surface improves all the parameters of the fine structure. Nevertheless, the conditions of $\rho>\rho_{\pm}$ and $\sigma_{sh}>\sigma_l$ are satisfied in the whole material. This means that after the wheel steel mark surface treatment, the lattice distortion is purely plastic, as in the initial state, and does not lead to the microcrack formation in the material.

Figure 7. Microstructure along the cross section of Wheel Steel Mark 2 after electrolyte-plasma surface hardening obtained by scanning electron microscope a) a hardened layer; b) a transition layer; c) non-hardened layer; d) general view

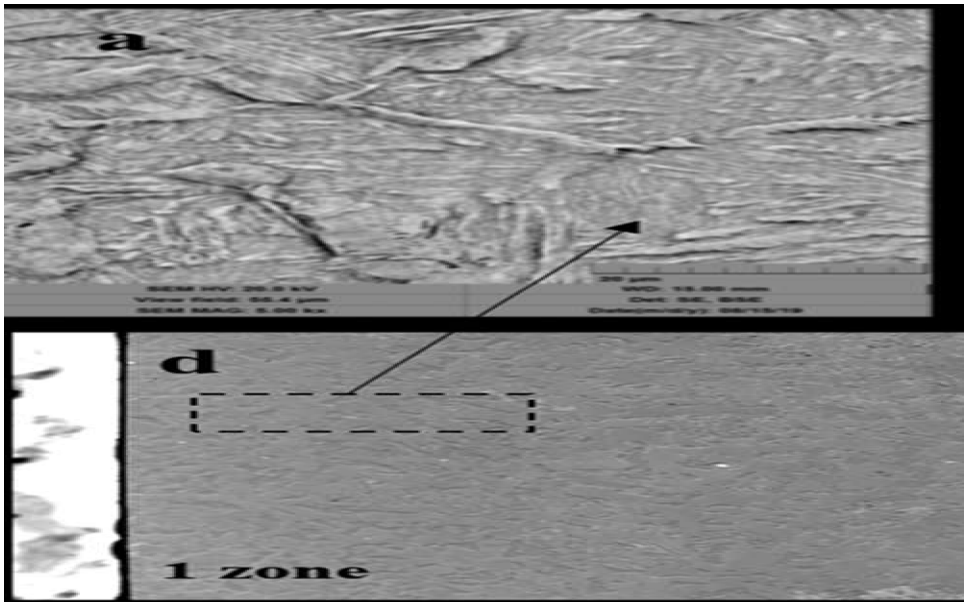

Figure 8. Microhardness over the cross section of wheel steel mark two after electrolytic plasma surface hardening

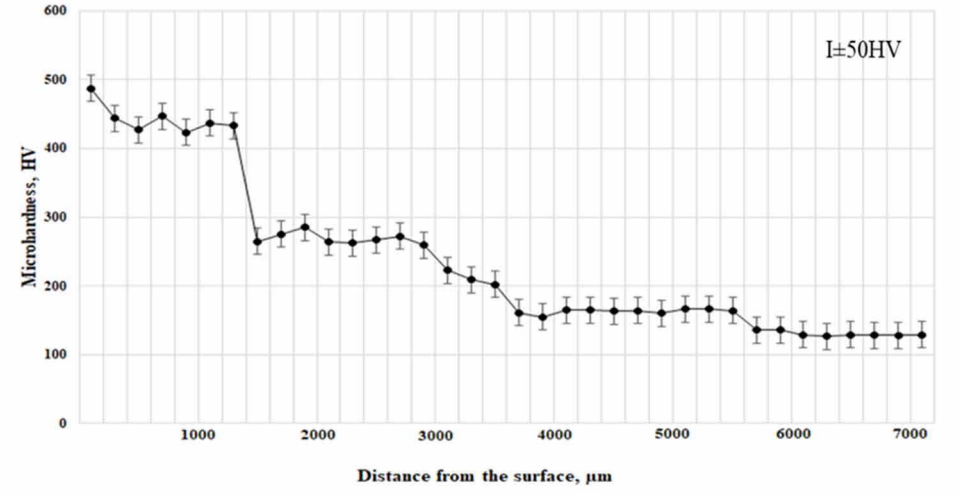

The research results show that electrolytic plasma quenching of the steel surface leads to the formation of the structure consisting of α- and γ-phases and $M_{23}C_6$ carbides. The wheel steel mark 2 represents a mixture of ferrite and carbide. However, according to TEM observations, this structure always contains the boundaries inherited from the martensite structure. Therefore, this structure can also be called lath and lamellar tempered martensite.

Figure 7 shows that the electrolyte-plasma surface hardening led to a change in the microstructure of the cross section, where the zoning of structures typical of electrolyte-plasma treatment is visible. The cross-sectional structure consists of 3 zones: 1 zone - a zone of surface hardening with a thickness of 1000-1500 μm, 2 zone - a zone of thermal influence, 3 zone - a matrix.

As is known, one of the most important properties of the surface layer, which significantly affects the strength characteristics, is microhardness, the value of which in the initial state (matrix) of steel mark 2 is ~ 140 HV. In this work, we studied the changes in the microhardness of a specimen of steel mark 2 over a cross section after electrolytic plasma surface hardening. According to the results obtained, the average microhardness in the surface hardening zone is ~ 420 HV, in the heat-affected zone it is ~ 260 HV and, accordingly, in the steel mark 2 matrix, the microhardness remains unchanged.

The development of promising technologies aimed at improving traditional and creating new methods of impact on the surface to give it the properties required by operating conditions is undoubtedly one of the urgent tasks of modern science and technology. Electrolytic plasma surface hardening, which is one of the varieties of plasma hardening, has recently been developed and intensively studied. This method is characterized by lower energy consumption, simplicity of technological equipment, and large dimensions of the hardened zone. The advantages of the method are a rather high productivity of the process and the ability to harden parts of large mass and complex profile, and the degree of hardening is comparable to plasma hardening. Practice shows that in order to extend the service life of heavily loaded parts and assemblies, surface plasma hardening is rational in terms of versatility, accessibility, environmental friendliness and economic efficiency.

CONCLUSION

This study results of phase composition, fine structure, and properties of wheel steel mark 2 before and after electrolyte-plasma surface hardening has shown that:

- In its initial state, matrix of wheel steel mark 2 represents α-phase the volume ratio of unfragmented ferrite is ~10% and 55% of fragmented one respectively and pearlite with a volume of ~ 35%.
- The morphological components of the structure of wheel steel mark 2 after EPSH are: martensite in the form of packet martensite with a volume fraction of 60%, lamellar low-temperature and lamellar high-temperature martensite's with volume fractions of ~ 10% and ~ 30%, respectively.

Electrolyte-plasma surface hardening of wheel steel led to:

- Martensite transformation, steel self-tempering (formation of cementite particles inside all martensite crystals), diffusion transformation of γ®α phases and release of residual austenite (γ-phase) along low-temperature martensite laths and lamellas and in all crystals of lamellar martensite.
- Formation of special carbide $M_{23}C_6$ particles due to decomposition of residual austenite and martensite, partial dissolution of cementite and carbon removal from α-phase crystal dislocations and boundaries, increase in all the parameters of the steel fine structure.

It was determined that electrolyte-plasma surface hardening leads to a change and hardening of the surface layer of wheel steel mark 2, the thickness of the hardened layer is ~ 1000-1500 μm, and the microhardness increases by ~ 3 times.

REFERENCES

Abuali, G. S., & Mousavi, S. M. (2013). Effect of pulse frequency on microstructure and surface properties of Ck45 steel treated by plasma electrolysis method. *Journal of Alloys and Compounds*, *551*, 415–421. doi:10.1016/j.jallcom.2012.10.176

Bayatanova, L., Rakhadilov, B., Kurbanbekov, S., Skakov, M., & Popova, N. (2021). Fine structure of low-carbon steel after electrolytic plasma treatment. *Materials Testing*, *63*(9), 842–847. doi:10.1515/mt-2020-0119

Grishunin, V. A. (2014). *Increasing the fatigue life of rail steel by electron beam processing*. [Dissertation of Candidate of Technical Sciences. Siberian State Industrial University, Novokuznetsk].

Kashchenko, M. P., Dzhemilev, K. N., & Chashchina, V. G. (2012). The connection of various habituses with variants of orientation relations under γ-α martensitic transformation in dynamic theory. Fundamental problems of modern. *Materials Science*, (1), 50–56.

Kondrat'ev, V. V., Balanovskii, A. E., Ivanov, N. A., Ershov, V. A., & Kornyakov, M. V. (2014). Evaluation of the Effect of Modifier Composition with Nanostructured Additives on Grey Cast Iron Properties. *Metallurgist*, *58*(5-6), 377–387. doi:10.100711015-014-9919-x

Konstantinova, M. V., Balanovskiy, A. E., Gozbenko, V. E., Kargapoltsev, S. K., Karlina, A. I., Shtayger, M. G., & Kuznetsov, B. O. (2019). Application of plasma surface quenching to reduce rail side wear. *IOP Conference Series. Materials Science and Engineering*, *560*(1), 012146. doi:10.1088/1757-899X/560/1/012146

Kozlov, E., Skakov, M., Uazyrkhanova, G., & Popova, N. (2014). Redistribution of second phase particles in surface layers of deformed roll. *Advanced Materials Research*, *1013*, 158–165. doi:10.4028/www.scientific.net/AMR.1013.158

Lobanov, M. L., Rusakov, G. M., Redikul'tsev, A. A., Belikov, S. V., Karabanalov, M. S., Struina, E. R., & Gervas'ev, A. M. (2016). Investigation of Special Misorientations in Lath Martensite of Low Carbon Steel Using the Method of Orientation Microscopy. *The Physics of Metals and Metallography*, *117*(3), 254–259. doi:10.1134/S0031918X1603008X

Nguyen, V. T., Astafeva, N. A., Tikhonov, A. G., Balanovskiy, A. E., & Vu, V. H. (2022). Evaluation of the Hardness and Wear Resistance of Alloyed Coatings From Fastening CuSn/CrxCy Mixture Hardened by Plasma and Laser. *Tribology in Industry*, *44*(3), 518–527. doi:10.24874/ti.1074.03.21.07

Paulmier, T., Bell, J. M., & Fredericks, P. M. (2008). Development of a novel cathodic plasma-electrolytic deposition technique. Part 2: Physico-chemical analysis of the plasma discharge. *Journal of Materials Processing Technology*, (208), 117–123. doi:10.1016/j.jmatprotec.2007.12.101

Popova, N. A., Nikonenko, E. L., Tabieva, E. E., & Uazyrkhanova, G. K. (2020). Structure and phase composition of ferritic-perlitic steel surface after electrolytic plasma quenching. *Russian Physics Journal*, *63*(5), 791–796. doi:10.100711182-020-02099-z

Popova, N. A., Nikonenko, E. L., Tabieva, E. E., Uazyrkhanova, G. K., & Gromov, V. E. (2020). Influence of surface quenching on morphology and phase composition of ferritic-pearlitic steel. *Izvestiya Ferrous Metallurgy*, *63*(11-12), 915–921. doi:10.17073/0368-0797-2020-11-12-915-921

Rahadilov, B. K., Zhurerova, L. G., Sagdoldina, Z. B., Kenesbekov, A. B., & Bayatanova, L. B. (2021). Morphological Changes in the Dislocation Structure of Structural Steel 20GL after Electrolytic-Plasma Hardening of the Surface. *Journal of Surface Investigation. X-ray, Synchrotron and Neutron Techniques*, *15*(2), 408–413. doi:10.1134/S1027451021020300

Rakhadilov B. K., Baizhan D. R., Uazyrkhanova G. K. & Tabieva Y.Y. (2020). *Patent for utility model No. 5365.* State Register of Utility Models of the Republic of Kazakhstan.

Rakhadilov, B. K., Buranich, V. V., Satbayeva, Z. A., Kozhanova, R. S., & Pogrebnjak, A. D. (2020). The cathodic electrolytic plasma hardening of the 20Cr2Ni4A chromium-nickel steel. *Journal of Materials Research and Technology*, *9*(4), 6969–6976. doi:10.1016/j.jmrt.2020.05.020

Rakhadilov, B. K., Tabieva, E. E., & Zhurerova, L. G. (2019). Plasma-electrolytic Nitriding of 0.3Cr-1Mn-1Si-Fe Construction Steel. *METAL 2019 - 28th International Conference on Metallurgy and Materials, Conference Proceedings*, (pp. 1174-1179). Research Gate.

Rakhadilov, B. K., Tabiyeva, Y. Y., Uazyrkhanova, G. K., Zhurerova, L. G., Maulit, A., & Baizhan, D. (2019). Surface modification of steel mark 2 electrolytic-plasma exposure. *Eurasian Journal of Physics and Functional Materials*, (3), 355–362.

Rakhadilov, B. K., Zhurerova, L. G., & Pavlov, A. V. (2016). Electrolyte-plasma surface hardening of 65G and 20GL low-alloy steels. *Bulletin of the University of Karaganda*, *4*(84), 8–13.

Rakhadilov, B. K., Zhurerova, L. G., Scheffler, M., & Khassenov, A. K. (2018). Change in high-temperature wear resistance of high-speed steel by plasma nitriding. *Bulletin of the University of Karaganda*, *3*(91), 59–65.

Skakov, M. K., Uazyrkhanova, G. K., & Popova, N. A. (2013). Electron microscopic analysis of 30CrMnSiA steel surface layers after hot deformation. *Applied Mechanics and Materials*, *395-396*(396), 336–340. doi:10.4028/www.scientific.net/AMM.395-396.336

Tabieva, E. E., Zhurerova, L. G., & Baizhan, D. (2020). Influence of Electrolyte-Plasma Hardening Technological Parameters on the Structure and Properties of Banding Steel 2. *Key Engineering Materials*, *839*, 57–62. doi:10.4028/www.scientific.net/KEM.839.57

Wang, L., Pyzalla, A., Stadlbauer, W., & Werner, E. A. (2003). Microstructure features on rolling surfaces of railway rails subjected. *Materials Science and Engineering A*, *359*(1-2, A359), 31–43. doi:10.1016/S0921-5093(03)00327-7

Zhang, P., Nie, X., & Northwood, D. O. (2009). Influence of coating thickness on the galvanic corrosion properties of Mg oxide in an engine coolant. *Surface and Coatings Technology*, *203*(20-21), 3271–3277. doi:10.1016/j.surfcoat.2009.04.012